

# Spin excitations in $\text{Nd}_{1-x}\text{Sr}_x\text{NiO}_2$ and $\text{YBa}_2\text{Cu}_3\text{O}_{7-\delta}$ : the influence of Hubbard $U$

F. Rosa,<sup>1,\*</sup> L. Martinelli,<sup>1,†</sup> G. Krieger,<sup>2,‡</sup> L. Braicovich,<sup>3</sup> N.B. Brookes,<sup>3</sup> G. Merzoni,<sup>1,4</sup> M. Moretti Sala,<sup>1</sup> F. Yakhou-Harris,<sup>3</sup> R. Arpaia,<sup>5,6</sup> D. Preziosi,<sup>2</sup> M. Salluzzo,<sup>7</sup> M. Fidrysiak,<sup>8</sup> and G. Ghiringhelli<sup>1,9,§</sup>

<sup>1</sup>*Dipartimento di Fisica, Politecnico di Milano, piazza Leonardo da Vinci 32, I-20133 Milano, Italy*

<sup>2</sup>*Université de Strasbourg, CNRS, IPCMS UMR 7504, F-67034 Strasbourg, France*

<sup>3</sup>*ESRF, The European Synchrotron, 71 Avenue des Martyrs, CS 40220, F-38043 Grenoble, France*

<sup>4</sup>*European XFEL, Holzkoppel 4, Schenefeld, D-22869, Germany*

<sup>5</sup>*Quantum Device Physics Laboratory, Department of Microtechnology and Nanoscience, Chalmers University of Technology, SE-41296 Göteborg, Sweden*

<sup>6</sup>*Department of Molecular Sciences and Nanosystems, Ca' Foscari University of Venice, I-30172 Venice, Italy*

<sup>7</sup>*CNR-SPIN, Complesso Monte Sant'Angelo-Via Cinthia, I-80126 Napoli, Italy*

<sup>8</sup>*Institute of Theoretical Physics, Jagiellonian University, ul. Lojasiewicza 11, PL-30348 Kraków, Poland*

<sup>9</sup>*CNR-SPIN, Dipartimento di Fisica, Politecnico di Milano, I-20133 Milano, Italy*

(Dated: June 14, 2024)

We use Resonant Inelastic X-ray Scattering (RIXS) to compare the doping dependence of magnetic excitations of an Infinite-Layer nickelate to those of a prototypical superconducting cuprate. The polarization analysis of RIXS spectra establishes the dominant spin-flip nature of the mid-infrared peak in both cases. Hole doping leads to opposite behavior of the magnetic energy in the two materials. By fitting the data with an original Hubbard-based model for dynamic susceptibility, we find that  $t$  is comparable in the two materials while  $U$  is about twice larger in the nickelate. This finding accounts for the smaller magnetic bandwidth of nickelates and for its decrease upon doping.

**DOI:**

*Introduction* – In high- $T_c$  superconducting cuprates the ground state and the transport properties are determined by an intricate tangle of orbital, charge, spin and lattice degrees of freedom [1–9]. Consequently, a consensus on how to properly describe their superconducting (SC) and normal state properties is still missing despite three decades of experimental and theoretical efforts. The problem can be attacked indirectly by replicating the physics of cuprates in other materials. Infinite-Layer (IL) nickelates are particularly well suited to this task [10–13]. Indeed, the  $3d^9$  spin- $\frac{1}{2}$  square-lattice of  $\text{Cu}^{2+}$  ions is mimicked by  $\text{Ni}^{1+}$  ions in  $\text{R}_{(1-x)}\text{Sr}_x\text{NiO}_2$  (R stands of La, Nd or Pr), leading to superconductivity [14] and to electronic properties that can be conveniently compared to cuprates.

The planar square coordination is required for the chemical stabilization of the monovalent  $\text{Ni}^{1+}$  ion [13, 15–17] and ensures that, by removing the degeneracy between the two  $e_g$  states, the  $\text{Ni}^{2+}$  hole-doped sites are in a low-spin configuration compatible with superconductivity [18]. This quasi-2D structure can only be achieved in infinite-layer ultra-thin films, obtained by de-intercalating apical oxygen atoms from pristine perovskite structure [19–26]. Notwithstanding several affinities in their temperature-doping ( $T/p$ ) phase diagrams [27, 28], IL nickelates show some remarkable differences [29] with respect to cuprates. Firstly, the charge-transfer energy  $\Delta$  is larger, therefore confining doping holes on Ni  $3d$  orbitals [17, 18, 30]. Secondly, the rare-earth atom plays a more significant role than in cuprates [16, 31, 32],

providing pockets of  $5d$  states close to the Fermi level. While these  $5d$  electron pockets are little hybridized with Ni  $3d_{x^2-y^2}$  states [33], thus minimally affecting antiferromagnetic correlations in the  $\text{NiO}_2$  planes, they can provide self-doped holes even in the undoped  $\text{RNiO}_2$  [34]. This self-doping might explain the report of superconductivity in nominally undoped  $\text{LaNiO}_2$  [33].

Muon-spin rotation measurements provided evidence of coexisting magnetism and SC [35]. Moreover, the dispersion of spin excitations measured by Resonant Inelastic X-ray Scattering (RIXS) indicated the robust settling of antiferromagnetic correlations in the  $\text{NiO}_2$  planes, although the characteristic energy of damped magnons (paramagnons) softens as a function of doping [36, 37], contrary to cuprates [38]. This softening was attributed to the spin dilution effect, i.e., a decrease in the average spin moment due to the introduction of doped holes on Ni sites. However, a clear description of the phenomenon was hindered by the difficulty in disentangling the coherent spin response from electron-hole excitations.

In this letter, by using polarization-resolved RIXS we are able to single-out magnetic and charge excitations in the low energy region of undoped and Sr-doped  $\text{NdNiO}_2$  and of antiferromagnetic and Ca-doped  $\text{YBa}_2\text{Cu}_3\text{O}_{7-\delta}$  (YBCO). We confirm the magnetic nature of the mid-infrared excitation in IL-nickelates and the softening of paramagnons in doped samples. Besides the usual damped harmonic oscillator fit, we analyze the spectral shape with a Hubbard-type theoretical model allowing the determination of both the hopping integral  $t$  and the

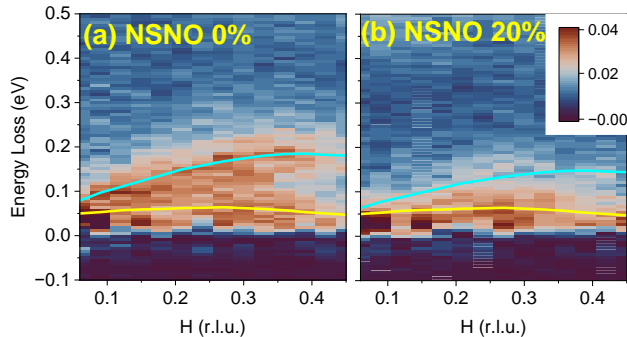


FIG. 1. Energy loss/momentum maps of  $\text{Nd}_{1-x}\text{Sr}_x\text{NiO}_2$ , for the two doping levels  $x = 0$  (a) and  $x = 0.2$  (b). The intensity scale is the same, shown in the (b) inset. The elastic peak has been subtracted for convenience. Yellow and cyan lines are eye guides for the phonon and magnon peak respectively.

Coulomb repulsion  $U$  [11, 39, 40]. We demonstrate that a smaller  $t/U$  ratio can explain the narrower magnetic bandwidth of nickelates with respect to cuprates even without invoking spin dilution.

*Experimental details* – RIXS spectra were measured at the beamline ID32 of the European Synchrotron (ESRF) in Grenoble, France [41]. The combined resolution at the Ni  $L_3$  edge (854.3 eV) was 39 meV, while at Cu  $L_3$  (931 eV) it was 30 and 40 meV for spectra without and with polarization analysis respectively. The scattering angle  $2\theta$  was fixed at  $149.5^\circ$  and the incident radiation was linearly polarized in the horizontal scattering plane ( $\pi$  polarization), so to enhance the spin-flip excitations for positive values of the momentum transfer, i.e., for grazing emission geometry. Momentum-resolved measurements were carried out on both samples along the  $(H,0)$  direction of the Brillouin zone. The spin-flip nature of the various features was assessed by measuring the two linear polarization components  $\pi'$  and  $\sigma'$  of the scattered radiation thanks to the polarimeter installed on the ERIXS spectrometer [41, 42]. The temperature was set to 20 K in order to minimize anti-Stokes signal and radiation damage of the samples. We performed measurements on 9 nm-thick films of  $\text{Nd}_{1-x}\text{Sr}_x\text{NiO}_2$  (hereafter NSNO), with doping levels of  $x = 0$  (undoped) and 0.2 (optimally doped). Both samples were obtained from pristine  $\text{Nd}_{1-x}\text{Sr}_x\text{NiO}_3$  perovskite films grown by Pulsed Laser Deposition (PLD) on  $\text{SrTiO}_3(001)$  (STO) single crystals substrate, and capped with three unit cells of STO. The perovskite was then reduced to the IL structure via a soft-chemistry process as described in ref. 43. The sample preparation was carried out at IPCMS, Strasbourg, France. As cuprate reference, we used  $\text{YBa}_2\text{Cu}_3\text{O}_{7-\delta}$ : one 150 nm-thick film was grown on a  $(110)$   $(\text{LaAlO}_3)_{0.3}(\text{Sr}_2\text{TaAlO}_6)_{0.7}$  (LSAT) substrate; this sample was almost perfectly undoped with  $\delta \simeq 1$  ( $p \simeq 0.03$ , referred to hereafter as YBCO 0%). Another

100 nm-thick film, grown on  $(001)$  STO, was fully oxygenated, with  $T_c \simeq 88$  K and  $\delta = 0$  ( $p = 0.19$ , YBCO 19%). Polarimetric measurements were performed on the same YBCO 19% at  $T = 80$  K and on another 100 nm-thick,  $(001)$  STO-grown underdoped YBCO film, with  $T_c \simeq 63$  K and  $\delta \simeq 0.3$  ( $p \simeq 0.13$ , YBCO 13%). The latter was measured at  $T = 60$  K. YBCO samples were grown by PLD at Chalmers University, Sweden [44].

*Results and discussion* – Fig. 1 reports the energy/momentum RIXS intensity maps of NSNO 0% and NSNO 20% along the  $(H,0)$  in-plane direction of the reciprocal space. The undoped sample shows a peak dispersing up to  $\sim 200$  meV, which is assigned to a spin wave excitation (magnon) [36, 37], marked by the light-blue line as a guide to the eye. The feature is much broader for the NSNO 20% so that the dispersion is harder to visualize. This effect can be attributed, as in cuprates [45], to magnetic disorder in the doped samples [36, 37]. In Figures 2(a)-(b) we compare RIXS spectra of NSNO and YBCO at the same doping level. We can notice the broadening and overall softening of the orbital excitations (between 0.5 eV and 3 eV) upon doping, consistently with previous observations [17, 46]. In YBCO the shift of the  $dd$  peaks looks smaller than in the IL nickelate, but with a larger broadening. We can explain this by the different nature of the doping holes: in cuprates, the relatively small value of the charge-transfer  $\Delta$  drives them into the oxygen band, without affecting significantly the energy of copper orbitals. Conversely, in NSNO the positive carriers are added to the Ni  $3d$  states, thus contributing to the downward shift of the Fermi level on Ni bands [16, 17].

In order to compare quantitatively the spin excitations in the four samples, we fitted the spectra with the damped harmonic oscillator (DHO) model previously used for cuprates [45] and IL nickelates [36]. As shown in Fig. 2(c-d), we fitted also the elastic peak and one phonon with resolution-wide Gaussian function, and a very broad Gaussian for the tail of the high-energy electronic excitations. The momentum dependence of the undamped energy  $\omega_0$  and damping coefficient  $\gamma$  of the magnon/paramagnon are shown in panels (e-f).

The dispersion curves of magnetic excitations exhibit a similar shape across all samples. However, in the infinite-layer (IL) nickelates, the curve is located at approximately half the energy of the cuprates, indicating a smaller nearest-neighbor superexchange interaction [36]. Additionally, the magnetic peak evolves differently with doping in these materials: in IL nickelates, the energy decreases with doping, whereas in cuprates it increases, consistently with previous findings [36, 45]. Furthermore, the damping grows with doping in YBCO, while it remains unchanged within the statistical confidence range in NSNO. In cuprates the increase of the spin excitation energy upon hole doping is attributed to the three-site term enabled by neighboring doped sites, which overcompensates the reduction of the average spin moment

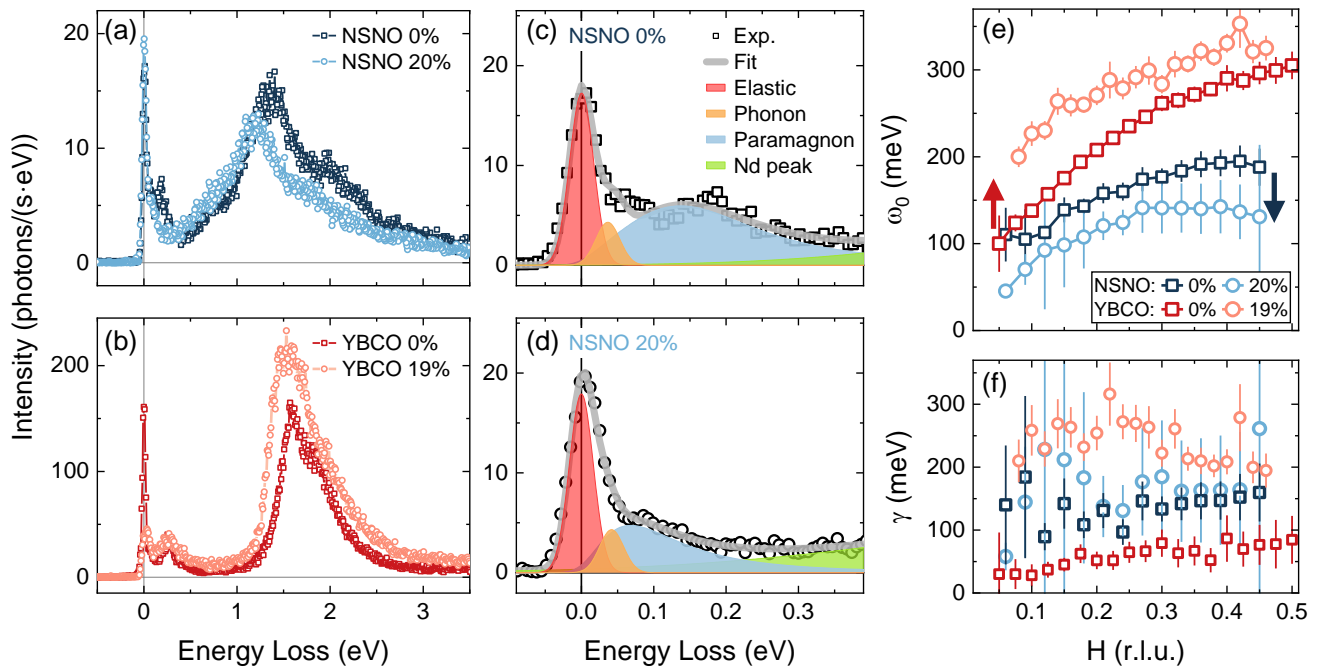


FIG. 2. Selected RIXS spectra of NSNO at  $\mathbf{Q} = (0.36, 0)$  (a) and YBCO 0% at  $\mathbf{Q} = (0.35, 0)$  and 19% at  $\mathbf{Q} = (0.36, 0)$  respectively. (b). Fitting of the low-energy region, using the damped harmonic oscillator model for the paramagnon for NSNO 0% (c) and 20% (d). The tail of the Nd hybridization peak (green curve) also includes charge continuum and dd contributes. The momentum dependence of the undamped frequency  $\omega_0$  and damping coefficient  $\gamma$  are presented in panels (e) and (f) respectively.

[38], and the increase in the damping is justified in terms of shortening of the spin-spin correlation function upon doping (increased spin disorder). How can we explain the different behavior of IL-nickelates? With the aim of solving these shortcomings, we decided to go beyond the DHO by measuring more accurately the spectral shape of the spin excitations and by analysing it with a more advanced model.

*Polarimeter analysis* – The broadness of the spin excitations in the doped sample makes it hard to single-out pure spin-flip excitations from the spin-conserving ones (e.g. bimagnons). Single-magnon excitations have pure crossed polarization character, because they imply the transfer of one unit of angular momentum from the scattering photon to the sample, i.e., a  $90^\circ$  rotation of the linear polarization of the x-ray photon [38, 47–49]. Therefore, we performed a polarization analysis of the scattered x-rays [46, 50], which is shown in Fig. 3. For NSNO 0% and YBCO 13% and 19%, the 200-300 meV peaks linked to magnetic excitations have almost pure crossed character ( $\pi, \sigma'$ ), while the intensity of the parallel polarization spectrum ( $\pi, \pi'$ ), mostly due to spin-conserving charge excitations (electron-hole pairs) and to bimagnons, is much weaker and featureless. The dd excitations exhibit different trends well described by single-ion model calculations [46, 50]. The polarimetric analysis

allows us to extract the pure spectral shape of the spin excitations, otherwise strongly mixed with the tail of the elastic and phonon peak in the unpolarized spectrum, thus enabling a more accurate analysis with theoretical models.

*Microscopic model of magnetic excitations* – Having obtained the pure spin part of the mid-infrared range spectrum, we carry out a microscopic analysis by employing a layered square-lattice Hamiltonian  $\mathcal{H} \equiv \sum_{i \neq j} t_{ij} \hat{a}_{i\sigma}^\dagger \hat{a}_{j\sigma} + U \sum_i \hat{n}_{i\uparrow} \hat{n}_{i\downarrow} + \frac{1}{2} \sum_{i \neq j} V_{ij} \hat{n}_i \hat{n}_j$ , extending two-dimensional Hubbard model recently proposed as a unifying framework describing low-energy electronic states of both Cu and Ni based superconductors [39]. To address multi- and infinite-layer systems, we select equal in-plane and out-of-plane lattice constants. The model is analyzed using the variational wave function approach combined with  $1/\mathcal{N}_f$  expansion (VWF+ $1/\mathcal{N}_f$ ) [51, 52], see Supplemental Material (SM) [53]. The free microscopic parameters are the on-site Coulomb repulsion  $U$ , the in-plane nearest- and next-nearest-neighbor hopping integrals ( $t$  and  $t'$ ), the screened intersite Coulomb interactions  $V_{ij}$ , and the hole-doping  $\delta$ . From DFT + DMFT (Dynamical Mean Field Theory) calculations the estimated values of  $t$  and  $t'$  are comparable in cuprates and IL-nickelates [39], whereas the effective value of  $U$  is expected to differ by a factor  $\sim 2$  as it is constrained by the

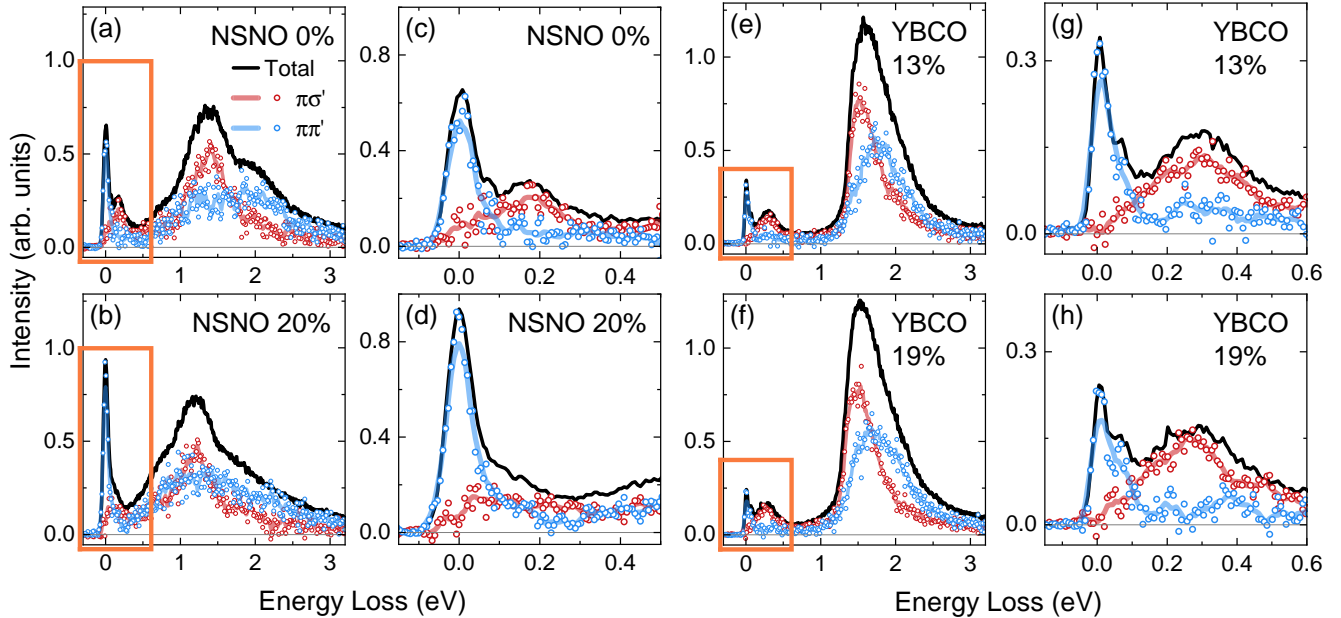


FIG. 3. Polarization-resolved spectra of NSNO (a)-(d) at  $\mathbf{Q} = (0.36, 0)$ , and YBCO (e)-(h) at  $\mathbf{Q} = (0.44, 0)$ . The solid black line is the average of the crossed polarization ( $\pi\sigma'$ , red dots) and parallel polarization spectra ( $\pi\pi'$ , blue dots). The solid blue and red lines show spectra smoothings over 7 points.

experimental paramagnon bandwidth  $\propto \frac{4t^2}{U}$ . Microscopically, such variation of  $U$  has been interpreted in terms of distinct one-band model mapping for charge-transfer and Mott-Hubbard insulators [11, 54]. Hereafter we refer to  $U/|t| \sim 6$ -8 and  $U/|t| \gtrsim 9$  as cuprate- and nickelate regimes, respectively. The role of  $V_{ij}$  terms is to suppress phase-separation, and they are determined as a solution of generalized lattice Poisson equation [53].

In Fig. 4(a) we compare the hole-doping evolution of the calculated dissipative part of dynamical spin susceptibility  $\chi''_s(\omega, \mathbf{Q})$  at  $\mathbf{Q} = (H, K) = (0.36, 0)$  r.l.u. for  $U = 6|t|$  (red) and  $U = 11|t|$  (blue), both with the same hopping integrals ( $t = -0.4$  eV,  $t' = 0.25|t|$ ) and non-local Coulomb terms. The temperature is set to  $k_B T = 0.35|t| \sim 0.12$  eV so as to stabilize the paramagnetic state and preserve the physical hierarchy  $k_B T \lesssim \omega_0, \gamma$ . Note that the simulated spectra separate into a resonant low-energy paramagnon peak and a featureless particle-hole continuum, extending to larger energies, which goes beyond the DHO-model phenomenology. The  $U = 6|t|$  solution contains a robust paramagnon centered at  $\approx 0.3$  eV, in agreement with previous theoretical studies of magnetic excitations in doped cuprates [52, 55, 56]. On the other hand, in the nickelate regime (blue curves) the paramagnons *are not* robust and we observe a crossover from a well-defined peak at  $\delta = 10\%$  to a broader asymmetric lineshape at  $\delta \gtrsim 20\%$ . *This suggests that the magnitude of the effective  $U$  is the principal microscopic factor differentiating the observed doping*

Parameter	Cuprate	Nickelate
$t$	-0.35 eV	-0.4 eV
$U$	$7 t  = 2.45$ eV	$11 t  = 4.4$ eV
$t'$	$0.25 t $	$0.25 t $
$k_B T$	$0.35 t $	$0.3 t $
$\delta$	0.13	0.1, 0.2

TABLE I. Microscopic Hubbard parameters obtained by fitting the polarimetric experimental data of YBCO 13%, NSNO 0% and NSNO 20% with the theoretical dynamical spin susceptibility.

*evolutions of the magnetic excitations.*

We fitted the polarimetric cross-polarized spectra of YBCO 13%, NSNO 0% and NSNO 20% with the theoretical dynamical spin susceptibilities (Fig. 4(b)-(d)), arriving at the parameters listed in Table I. Details of the microscopic-model analysis are presented in the SM [53]. The Mott self-energy for nickelates  $U \sim 4.4$  eV falls in between metallic nickel and NiO [11] and is in agreement with previous works [11, 39, 40, 57]. To account for self-doping, we assume a nonlinear dependence of  $\delta$  on the Sr concentration  $x$  in NSNO, as suggested by recent DFT+DMFT calculations [39], namely  $\delta = 0.1$  for NSNO 0%, and  $\delta = 0.2$  for NSNO 20%. We emphasize that for the two nickelate dopings all parameters are identical except  $\delta$  and that the same value of  $t'/t$  can be used for

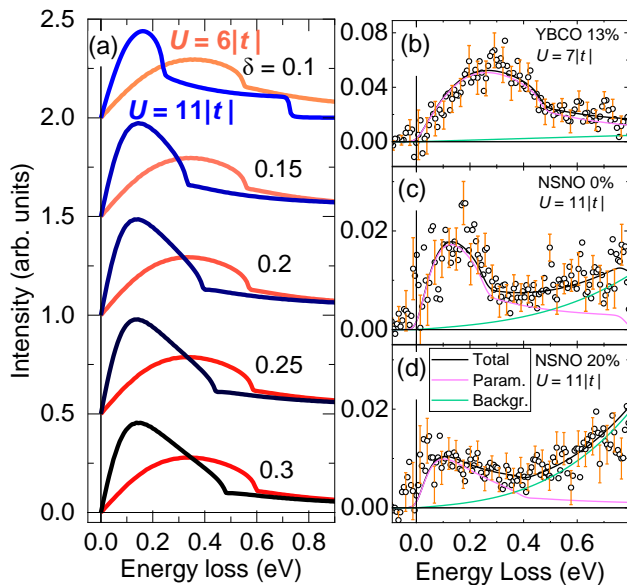


FIG. 4. (a): Theoretical dissipative parts of Hubbard-model susceptibilities  $\chi''(\mathbf{Q}, \omega)$  at  $\mathbf{Q} = (0.36, 0)$  for various doping levels  $\delta$ ; pink-red curves refer to the cuprate regime ( $U = 6|t|$ ), blue-black curves to nickelate regime ( $U = 11|t|$ ). The remaining parameters are:  $t = -0.4$  eV,  $t' = 0.25|t|$ ,  $k_B T = 0.35|t|$ . Theoretical susceptibilities were convolved with a 39 meV FWHM Gaussian to account for experimental resolution. (b): Low-energy fit of YBCO 13% cross-polarized spectrum (empty dots) at  $\mathbf{Q} = (0.44, 0)$  using our magnetic susceptibility (pink curves) plus a cubic background (aquamarine). (c)-(d): Same for NSNO 0% and 20% respectively, at  $\mathbf{Q} = (0.36, 0)$ . Microscopic parameters are reported in Table I for the two regimes.

YBCO and NSNO data. The latter finding is particularly relevant because  $t'/t$  is known to heavily affect the shape of the susceptibility and because the literature is not univocal on this point, with some authors proposing higher values of  $t'/t \sim 0.3 - 0.4$  [15, 57] and others using values comparable to ours [11, 39, 58]. We notice that fitting the spectra without polarization analysis would lead to smaller  $t'/t \sim 0.15$ , see Fig. 2 of SM [53]. The crucial role played by polarization-resolved analysis in this discernment is apparent. It is proved that the magnon softening in nickelates comes as a consequence of the smaller  $t/U$  ratio (see Fig. 4 (a)), giving further support to our model with no need of involving spin dilution effects, as previously proposed [36].

*Conclusions and perspectives* – By comparing the RIXS spectra of IL nickelates (NSNO) and cuprates (YBCO), both in undoped and doped states, we have highlighted the distinct doping dependence of magnetic excitations in these two families of quantum materials, in terms of both energy and damping. To further investigate these differences, the polarization-resolved RIXS spectra of NSNO revealed two key findings: i) the pres-

ence of a significant non-crossed component, detectable even in the nominally undoped sample, likely due to self-doping; and ii) the accurate shape of the pure magnetic response, which can be properly fitted with theoretical models going beyond the commonly used DHO model. Using our Hubbard-based approach, we successfully reproduced the different evolution of the dynamic spin response with doping in cuprates and nickelates, yielding reliable estimates of crucial parameters, such as the Mott-Hubbard  $U$  ( $\sim 2.45$  eV in YBCO and  $\sim 4.4$  eV in NSNO).

In this context, the role of the charge transfer  $\Delta$  remains to be clarified. As cuprates and IL nickelates are charge-transfer ( $\Delta < U$ ) and Mott-Hubbard ( $\Delta > U$ ) insulators, respectively,  $\Delta$  is expected to have significantly different values between the two materials. Such a hypothesis calls for further investigation, starting from the expected decrease of the exchange coupling  $J$  when  $\Delta$  is increased [59].

F.R., L.M., M.M.S., M.S. and G.G. acknowledge support by the projects PRIN2017 “Quantum-2D” ID 2017Z8TS5B and PRIN 2020 “QT-FLUO” ID 20207ZXT4Z of the Ministry for University and Research (MIUR) of Italy. R.A. acknowledges support by the Swedish Research Council (VR) under the Project 2020-04945. M.F. acknowledges support by grants Miniatura No. DEC-2021/05/X/ST3/00666 and Opus No. UMO-2021/41/B/ST3/04070 from Narodowe Centrum Nauki (NCN). D.P. acknowledges support from the project ANR-JCJC FOXIES (ANR-21-CE08-0021). For the purpose of Open Access, the author has applied a CC-BY public copyright licence to any Author Accepted Manuscript (AAM) version arising from this submission. This research used ESRF beam line ID32 under the proposals HC4831, HC5221 and HC5222. This work was performed in part at Myfab Chalmers.

\* francesco1.rosa@polimi.it

† Present address: Physik-Institut, Universität Zürich, Winterthurerstrasse 190, CH-8057 Zürich, Switzerland

‡ Present address: Eindhoven University of Technology, P.O. Box 513, 5600 MB Eindhoven, The Netherlands

§ giacomo.ghiringhelli@polimi.it

- [1] B. Keimer, S. A. Kivelson, M. R. Norman, S. Uchida, and J. Zaanen, From quantum matter to high-temperature superconductivity in copper oxides, *Nature* **518**, 179 (2015).
- [2] D. J. Scalapino, A common thread: The pairing interaction for unconventional superconductors, *Rev. Mod. Phys.* **84**, 1383 (2012).
- [3] E. Fradkin, S. A. Kivelson, and J. M. Tranquada, Colloquium: Theory of intertwined orders in high temperature superconductors, *Rev. Mod. Phys.* **87**, 457 (2015).
- [4] C. Proust and L. Taillefer, The remarkable underlying ground states of cuprate superconductors, *Annual Review of Condensed Matter Physics* **10**, 409 (2019).

- [5] C. Weber, C. Yee, K. Haule, and G. Kotliar, Scaling of the transition temperature of hole-doped cuprate superconductors with the charge-transfer energy, *Europhysics Letters* **100**, 37001 (2012).
- [6] A. Foley, S. Verret, A.-M. Tremblay, and D. Senechal, Coexistence of superconductivity and antiferromagnetism in the hubbard model for cuprates, *Physical Review B* **99**, 184510 (2019).
- [7] J. Zaanen, G. Sawatzky, and J. Allen, Band gaps and electronic structure of transition-metal compounds, *Physical Review Letters* **55**, 418 (1985).
- [8] J. Zaanen and G. Sawatzky, Systematics in band gaps and optical spectra of 3d transition metal compounds, *Journal of Solid State Chemistry* **88**, 8 (1990).
- [9] E. Wahlberg, R. Arpaia, G. Seibold, M. Rossi, R. Fumagalli, E. Trabeldo, N. B. Brookes, L. Braicovich, S. Caprara, U. Gran, *et al.*, Restored strange metal phase through suppression of charge density waves in underdoped  $\text{YBa}_2\text{Cu}_3\text{O}_{7-\delta}$ , *Science* **373**, 1506 (2021).
- [10] Y. Nomura and R. Arita, Superconductivity in infinite-layer nickelates, *Reports on Progress in Physics* **85**, 052501 (2022).
- [11] E. Been, W.-S. Lee, H. Y. Hwang, Y. Cui, J. Zaanen, T. Devereaux, B. Moritz, and C. Jia, Electronic structure trends across the rare-earth series in superconducting infinite-layer nickelates, *Physical Review X* **11**, 011050 (2021).
- [12] A. S. Botana, V. Pardo, and M. R. Norman, Electron doped layered nickelates: Spanning the phase diagram of the cuprates, *Physical Review Materials* **1**, 021801 (2017).
- [13] V. Anisimov, D. Bukhvalov, and T. Rice, Electronic structure of possible nickelate analogs to the cuprates, *Physical Review B* **59**, 7901 (1999).
- [14] D. Li, K. Lee, B. Y. Wang, M. Osada, S. Crossley, H. R. Lee, Y. Cui, Y. Hikita, and H. Y. Hwang, Superconductivity in an infinite-layer nickelate, *Nature* **572**, 624 (2019).
- [15] A. S. Botana and M. R. Norman, Similarities and differences between lanio2 and cacuo2 and implications for superconductivity, *Physical Review X* **10**, 011024 (2020).
- [16] M. Hepting, D. Li, C. Jia, H. Lu, E. Paris, Y. Tseng, X. Feng, M. Osada, E. Been, Y. Hikita, *et al.*, Electronic structure of the parent compound of superconducting infinite-layer nickelates, *Nature Materials* **19**, 381 (2020).
- [17] M. Rossi, H. Lu, A. Nag, D. Li, M. Osada, K. Lee, B. Y. Wang, S. Agrestini, M. Garcia-Fernandez, J. Kas, *et al.*, Orbital and spin character of doped carriers in infinite-layer nickelates, *Physical Review B* **104**, L220505 (2021).
- [18] M. Jiang, M. Berciu, and G. A. Sawatzky, Critical nature of the ni spin state in doped ndnio2, *Physical Review Letters* **124**, 207004 (2020).
- [19] D. Preziosi, A. Sander, A. Barthélémy, and M. Bibes, Reproducibility and off-stoichiometry issues in nickelate thin films grown by pulsed laser deposition, *AIP Advances* **7** (2017).
- [20] K. Lee, B. H. Goodge, D. Li, M. Osada, B. Y. Wang, Y. Cui, L. F. Kourkoutis, and H. Y. Hwang, Aspects of the synthesis of thin film superconducting infinite-layer nickelates, *Apl Materials* **8** (2020).
- [21] X. Ding, C. C. Tam, X. Sui, Y. Zhao, M. Xu, J. Choi, H. Leng, J. Zhang, M. Wu, H. Xiao, *et al.*, Critical role of hydrogen for superconductivity in nickelates, *Nature* **615**, 50 (2023).
- [22] P. Puphal, B. Wehinger, J. Nuss, K. Küster, U. Starke, G. Garbarino, B. Keimer, M. Isobe, and M. Hepting, Synthesis and physical properties of lanio2 crystals, *Physical Review Materials* **7**, 014804 (2023).
- [23] T. Onozuka, A. Chikamatsu, T. Katayama, T. Fukumura, and T. Hasegawa, Formation of defect-fluorite structured ndnio x h y epitaxial thin films via a soft chemical route from ndnio 3 precursors, *Dalton Transactions* **45**, 12114 (2016).
- [24] M. Crespin, P. Levitz, and L. Gatineau, Reduced forms of lanio3 perovskite. part 1.—evidence for new phases:  $\text{La}_2\text{Ni}_2\text{O}_5$  and lanio2, *Journal of the Chemical Society, Faraday Transactions 2: Molecular and Chemical Physics* **79**, 1181 (1983).
- [25] M. Hayward, M. Green, M. Rosseinsky, and J. Sloan, Sodium hydride as a powerful reducing agent for topotactic oxide deintercalation: synthesis and characterization of the nickel (i) oxide lanio2, *Journal of the American Chemical Society* **121**, 8843 (1999).
- [26] M. Hayward and M. Rosseinsky, Synthesis of the infinite layer ni (i) phase ndnio2+ x by low temperature reduction of ndnio3 with sodium hydride, *Solid State Sciences* **5**, 839 (2003).
- [27] S. Zeng, C. S. Tang, X. Yin, C. Li, M. Li, Z. Huang, J. Hu, W. Liu, G. J. Omar, H. Jani, *et al.*, Phase diagram and superconducting dome of infinite-layer nd1-xsrnio2 thin films, *Physical Review Letters* **125**, 147003 (2020).
- [28] D. Li, B. Y. Wang, K. Lee, S. P. Harvey, M. Osada, B. H. Goodge, L. F. Kourkoutis, and H. Y. Hwang, Superconducting dome in nd1-xsrnio2 infinite layer films, *Physical Review Letters* **125**, 027001 (2020).
- [29] K.-W. Lee and W. Pickett, Infinite-layer lanio2: Ni1+ is not cu2+, *Physical Review B* **70**, 165109 (2004).
- [30] B. H. Goodge, D. Li, K. Lee, M. Osada, B. Y. Wang, G. A. Sawatzky, H. Y. Hwang, and L. F. Kourkoutis, Doping evolution of the mott–hubbard landscape in infinite-layer nickelates, *Proceedings of the National Academy of Sciences* **118**, e2007683118 (2021).
- [31] P. Jiang, L. Si, Z. Liao, and Z. Zhong, Electronic structure of rare-earth infinite-layer rnio2 ( $r = \text{la, nd}$ ), *Physical Review B* **100**, 201106 (2019).
- [32] J. Kapteghian and A. S. Botana, Electronic structure and magnetism in infinite-layer nickelates rnio2 ( $r = \text{la-lu}$ ), *Physical Review B* **102**, 205130 (2020).
- [33] M. Osada, B. Y. Wang, B. H. Goodge, S. P. Harvey, K. Lee, D. Li, L. F. Kourkoutis, and H. Y. Hwang, Nickelate superconductivity without rare-earth magnetism:(la,sr)nio2, *Advanced Materials* **33**, 2104083 (2021).
- [34] G.-M. Zhang, Y.-f. Yang, and F.-C. Zhang, Self-doped mott insulator for parent compounds of nickelate superconductors, *Physical Review B* **101**, 020501 (2020).
- [35] J. Fowlie, M. Hadjimichael, M. M. Martins, D. Li, M. Osada, B. Y. Wang, K. Lee, Y. Lee, Z. Salman, T. Prokscha, *et al.*, Intrinsic magnetism in superconducting infinite-layer nickelates, *Nature Physics* **18**, 1043 (2022).
- [36] H. Lu, M. Rossi, A. Nag, M. Osada, D. Li, K. Lee, B. Wang, M. Garcia-Fernandez, S. Agrestini, Z. Shen, *et al.*, Magnetic excitations in infinite-layer nickelates, *Science* **373**, 213 (2021).
- [37] G. Krieger, L. Martinelli, S. Zeng, L. E. Chow, K. Kummer, R. Arpaia, M. M. Sala, N. B. Brookes, A. Ariando, N. Viart, M. Salluzzo, G. Ghiringhelli, and D. Preziosi, Charge and spin order dichotomy in ndnio2 driven by the

- capping layer, *Phys. Rev. Lett.* **129**, 27002 (2022).
- [38] C. J. Jia, E. A. Nowadnick, K. Wohlfeld, Y. F. Kung, C.-C. Chen, S. Johnston, T. Tohyama, B. Moritz, and T. P. Devereaux, Persistent spin excitations in doped antiferromagnets revealed by resonant inelastic light scattering, *Nature Communications* **5**, 3314 (2014).
- [39] M. Kitatani, L. Si, O. Janson, R. Arita, Z. Zhong, and K. Held, Nickelate superconductors—a renaissance of the one-band hubbard model, *npj Quantum Materials* **5**, 59 (2020).
- [40] P. Worm, L. Si, M. Kitatani, R. Arita, J. M. Tomczak, and K. Held, Correlations tune the electronic structure of pentalayer nickelates into the superconducting regime, *Physical Review Materials* **6**, L091801 (2022).
- [41] N. B. Brookes, F. Yakhou-Harris, K. Kummer, A. Fondacaro, J. Cezar, D. Betto, E. Velez-Fort, A. Amorese, G. Ghiringhelli, L. Braicovich, R. Barrett, G. Berruyer, F. Cianciosi, L. Eybert, P. Marion, P. van der Linden, and L. Zhang, The beamline ID32 at the ESRF for soft X-ray high energy resolution resonant inelastic X-ray scattering and polarisation dependent X-ray absorption spectroscopy, *Nucl. Instrum. Methods Phys. Res., Sect. A* **903**, 175 (2018).
- [42] L. Braicovich, M. Minola, G. Dellea, M. Le Tacon, M. Moretti Sala, C. Morawe, J.-C. Peffen, R. Suprunangnet, F. Yakhou, G. Ghiringhelli, *et al.*, The simultaneous measurement of energy and linear polarization of the scattered radiation in resonant inelastic soft x-ray scattering, *Review of Scientific Instruments* **85** (2014).
- [43] G. Krieger, A. Raji, L. Schlur, G. Versini, C. Bouillet, M. Lenertz, J. Robert, A. Gloter, N. Viart, and D. Preziosi, Synthesis of infinite-layer nickelates and influence of the capping-layer on magnetotransport, *Journal of Physics D: Applied Physics* **56**, 024003 (2023).
- [44] R. Arpaia, E. Andersson, E. Trabeldo, T. Bauch, and F. Lombardi, Probing the phase diagram of cuprates with  $\text{yba}_2\text{cu}_3\text{o}_{7-\delta}$  thin films and nanowires, *Phys. Rev. Mater.* **2**, 024804 (2018).
- [45] Y. Y. Peng, E. W. Huang, R. Fumagalli, M. Minola, Y. Wang, X. Sun, Y. Ding, K. Kummer, X. J. Zhou, N. B. Brookes, B. Moritz, L. Braicovich, T. P. Devereaux, and G. Ghiringhelli, Dispersion, damping, and intensity of spin excitations in the monolayer  $(\text{Bi,Pb})_2(\text{Sr,L a})_2\text{CuO}_{6+\delta}$  cuprate superconductor family, *Phys. Rev. B* **98**, 144507 (2018).
- [46] R. Fumagalli, L. Braicovich, M. Minola, Y. Peng, K. Kummer, D. Betto, M. Rossi, E. Lefrançois, C. Morawe, M. Salluzzo, *et al.*, Polarization-resolved  $\text{l 3-edge}$  resonant inelastic x-ray scattering of orbital and spin excitations in  $\text{ndba}_2\text{cu}_3\text{o}_{7-\delta}$ , *Physical Review B* **99**, 134517 (2019).
- [47] L. Braicovich, M. M. Sala, L. Ament, V. Bisogni, M. Minola, G. Balestrino, D. Di Castro, G. De Luca, M. Salluzzo, G. Ghiringhelli, *et al.*, Momentum and polarization dependence of single-magnon spectral weight for  $\text{l 3-edge}$  resonant inelastic x-ray scattering from layered cuprates, *Physical Review B* **81**, 174533 (2010).
- [48] L. J. Ament, G. Ghiringhelli, M. M. Sala, L. Braicovich, and J. van den Brink, Theoretical demonstration of how the dispersion of magnetic excitations in cuprate compounds can be determined using resonant inelastic x-ray scattering, *Physical Review Letters* **103**, 117003 (2009).
- [49] M. Haverkort, Theory of resonant inelastic x-ray scattering by collective magnetic excitations, *Physical Review Letters* **105**, 167404 (2010).
- [50] M. M. Sala, V. Bisogni, C. Aruta, G. Balestrino, H. Berger, N. B. Brookes, G. De Luca, D. Di Castro, M. Grioni, M. Guarise, *et al.*, Energy and symmetry of  $\text{dd}$  excitations in undoped layered cuprates measured by  $\text{Cu L}_3$  resonant inelastic x-ray scattering, *New J. Phys.* **13**, 043026 (2011).
- [51] M. Fidrysiak and J. Spalek, Universal collective modes from strong electronic correlations: Modified  $1/\mathcal{N}_f$  theory with application to high- $T_c$  cuprates, *Phys. Rev. B* **103**, 165111 (2021).
- [52] M. Fidrysiak and J. Spalek, Unified theory of spin and charge excitations in high- $t$   $c$  cuprate superconductors: A quantitative comparison with experiment and interpretation, *Physical Review B* **104**, L020510 (2021).
- [53] See Supplemental Material at [URL will be inserted by publisher] for further information.
- [54] L. F. Feiner, J. H. Jefferson, and R. Raimondi, Effective single-band models for the high- $T_c$  cuprates. I. Coulomb interactions, *Phys. Rev. B* **53**, 8751 (1996).
- [55] F. Nilsson, K. Karlsson, and F. Aryasetiawan, Dynamically screened coulomb interaction in the parent compounds of hole-doped cuprates: Trends and exceptions, *Physical Review B* **99**, 075135 (2019).
- [56] M. Fidrysiak and J. Spalek, Robust spin and charge excitations throughout the high- $t$   $c$  cuprate phase diagram from incipient motttness, *Physical Review B* **102**, 014505 (2020).
- [57] E. Pavarini, I. Dasgupta, T. Saha-Dasgupta, O. Jepsen, and O. Andersen, Band-structure trend in hole-doped cuprates and correlation with  $t$   $c$  max, *Physical Review Letters* **87**, 047003 (2001).
- [58] Y. Nomura, M. Hirayama, T. Tadano, Y. Yoshimoto, K. Nakamura, and R. Arita, Formation of a two-dimensional single-component correlated electron system and band engineering in the nickelate superconductor  $\text{ndnio}_2$ , *Physical Review B* **100**, 205138 (2019).
- [59] Y. Wang, E. W. Huang, B. Moritz, and T. P. Devereaux, Magnon splitting induced by charge transfer in the three-orbital hubbard model, *Physical Review Letters* **120**, 246401 (2018).